

# Gamma irradiation effect on properties of modified graphene doped PVA nanocomposite films

Thaises Lima<sup>1\*</sup> , Filipe Diniz<sup>1</sup> , Elmo Araújo<sup>1</sup>  and Patrícia Araújo<sup>2</sup> 

<sup>1</sup>*Laboratório de Polímeros e Nanoestruturas, Departamento de Energia Nuclear, Universidade Federal de Pernambuco – UFPE, Recife, PE, Brasil*

<sup>2</sup>*Departamento de Engenharia Biomédica, Universidade Federal de Pernambuco – UFPE, Recife, PE, Brasil*

\*[thaises.lima@ufpe.br](mailto:thaises.lima@ufpe.br)

## Abstract

Gamma radiation effects on extrinsically electrical semiconducting polymer nanocomposite films of poly(vinyl alcohol) (PVA) and 0.5 wt% histidine-modified reduced graphene oxide (H-RGO) filler were evaluated. Thermogravimetric analysis showed thermal degradation stages of the films and UV-Vis analysis allowed the study of optical parameters. Optical band gap energy ( $E_g$ ) of PVA was shifted from 6.20 to 3.76 eV with the addition of H-RGO filler into the polymer matrix, while the electrical conductivity changed from  $10^{-11}$  (isolator) to  $10^{-6}$  (semiconductor) S/cm and PVA/H-RGO nanocomposite reached  $10^{-4}$  S/cm at 25 kGy gamma-radiation dose. PVA/H-RGO nanocomposite films are promising in a wide range of potential applications, such as bio and chemical sensors, catalysis, and active layers for optoelectronic devices.

**Keywords:** *electrical conductivity, gamma radiation, optical band gap, polymer composites, thermal analysis.*

**How to cite:** Lima, T., Diniz, F., Araújo, E., & Araújo, P. (2024). Gamma irradiation effect on properties of modified graphene doped PVA nanocomposite films. *Polímeros: Ciência e Tecnologia*, 34(4), e20240042. <https://doi.org/10.1590/0104-1428.20230106>

## 1. Introduction

Electrically conducting polymer materials are at the forefront of semiconductors research since they can be used in optoelectronics, capacitors, photovoltaics, UV-blockers, biosensors, and optical limiters applications<sup>[1-3]</sup>. Polyvinyl alcohol (PVA) and polyvinyl pyrrolidone (PVP) are among the most popular polymers due to their unique properties such as dielectric nature, adherence property, fast hydro-dissolution, and water solubility. The semi-crystalline nature of PVA and its ability to form hydrogen bonds make this polymer a suitable candidate in many industrial applications such as photovoltaic solid-state electrolytes<sup>[4,5]</sup>.

Gamma irradiation is used extensively in many areas of industry, medicine, military, research, and nuclear power production. However, gamma irradiation is known to affect the electrical, optical, and mechanical properties of polymers or polymer composites. These changes happen through different mechanisms, e.g. main chain scissions<sup>[6]</sup>, crosslinking<sup>[7]</sup>, grafting<sup>[8]</sup>, stable radicals formation<sup>[9]</sup>, crystallinity reduction<sup>[10]</sup>, and alteration in particle size of embedded loads<sup>[11]</sup>. Furthermore, evaluating the impact of high-energy radiation on polymer composites may be crucial when these materials are in use in challenging environments, such as nuclear power plants, aircraft, spacecraft, satellites, and other applications.

Numerous studies target graphene/polymer nanocomposites to investigate the effects of gamma radiation<sup>[12-14]</sup>. Poly(vinyl alcohol) (PVA) has become of special interest as a polymer matrix

for graphene nanocomposites due to its good physicochemical properties. PVA is a water-soluble, biocompatible synthetic polymer<sup>[15]</sup> capable of forming strong hydrogen-bonding interactions through its hydroxyl group. In this work, it was used graphene oxide covalently modified with the proteic amino acid histidine, and chemically reduced with cysteine, another proteic amino acid, to produce histidine-modified reduced graphene oxide (H-RGO). The aim is to present an extensive study of these composites focused on optoelectronic applications. These nanocomposite films were gamma-irradiated with doses of up to 100 kGy, and their thermal, optical, and electrical properties were assessed. The findings suggest that nanocomposite material has a good potential as a gamma radiation resistant electronic component, which might be very suitable for optoelectronics, avionics, and aerospace applications.

## 2. Materials and Methods

### 2.1 Materials

Intercalated graphite flakes, PVA (OH-terminated,  $M_n = 89-98$  kg.mol<sup>-1</sup>), Histidine, and L-cysteine were purchased from Sigma Aldrich. Sulfuric acid (H<sub>2</sub>SO<sub>4</sub>), nitric acid (HNO<sub>3</sub>), and ethanol were purchased from Cinética Química (Brazil). Potassium permanganate (KMnO<sub>4</sub>), sodium hydroxide (NaOH), and sodium nitrate (NaNO<sub>3</sub>) were purchased from Dinâmica Química

(Brazil). Hydrogen peroxide (H<sub>2</sub>O<sub>2</sub>) was purchased from VETEC. All reagents were of analytical grade and were used as supplied.

## 2.2 Methods

### 2.2.1 Preparation of modified and reduced graphene oxide (H-RGO)

Graphene oxide (GO) was obtained from intercalated graphite flakes through Hummer's chemical oxidation method<sup>[16,17]</sup>. GO covalent modification was prepared as described in previous studies<sup>[18,19]</sup> to obtain histidine-modified graphene oxide (H-GO). In brief, 0.5 g of GO was suspended in 50 mL of deionized water, and approximately 9 mmol of histidine was added under stirring. Aqueous NaOH (0.2 mol.L<sup>-1</sup>) was mixed with the suspension and left under stirring for 24 h at 80 °C. The product was filtered and dried in an oven at 60 °C for 24 h. Chemical reduction of H-GO was performed with L-cysteine<sup>[20]</sup>. H-GO (0.25 g) was added to 150 mL of deionized water. The suspension was sonicated (Ultrasonic probe Sonic Vibracell, 500 W) for 5 min at room temperature under 50% amplitude. Reducing agent L-cysteine (5 g) was added and the mixture was stirred for 72 h. After this time, 20 mL NaOH (1 M) was added, and the resulting mixture was filtered. The residue was washed with absolute ethanol and dried for 24 h at 60 °C to yield 0.21 g of the final product H-RGO. A scheme for H-RGO preparation is presented in Figure 1.

### 2.2.2 Nanocomposite films preparation

Composite films were prepared by casting solution method. An aqueous solution of PVA (10 w/v%) was heated at 90 °C for 1h. 10 mL of the aqueous suspension of H-RGO (0.5 wt%) was sonicated for 10 min at 50% amplitude and added to PVA hot solution. The resulting mixture was stirred for 24 hours at 90 °C. The suspension was then cast on Petri dishes and dried in a dry box at 27 °C. PVA and PVA/H-RGO (0.5 wt%) nanocomposite films with 10 µm thick were peeled off the dishes. The films were gamma irradiated in 25, 50, and 100 kGy doses (60Co, E<sub>γ</sub> ~ 1.25 MeV, dose rate ~ 1.6 kGy/h, CG 220 Excel Irradiator – MDS Nordion Gamma Cell, Canada) in air at room temperature (~27 °C). Here, it was used 0.5 wt% of H-RGO into the PVA matrix to obtain PVA/H-RGO nanocomposite films, since this filler concentration reached better dispersion in water resulting in homogeneous nanocomposite films, as described in earlier studies<sup>[19]</sup>.

## 3. Characterization

### 3.1 Fourier Transform Infrared (FTIR) spectroscopy

GO, H-GO, and H-RGO were analyzed through Fourier Transform Infrared (FTIR) Spectroscopy in a FTIR-4600, JASCO-Japan, equipped with an Attenuated Total Reflection accessory ATR ProOne (ZnSe Crystal). Experiments were performed with 32 scans, 4 cm<sup>-1</sup>, in the 4000 - 500 cm<sup>-1</sup> wavenumber range.

### 3.2 Thermogravimetry Analysis (TGA)

Thermogravimetry Analysis (TGA) were performed in a Simultaneous Thermal Analyzer (TGA/DSC2 STARE System - Mettler Toledo) in 70 microliters aluminum oxide crucibles under nitrogen flux (50 mL.min<sup>-1</sup>), in the 25-600 °C range, with heating rates (β) of 10 °C.min<sup>-1</sup>.

### 3.3 UV-Visible (UV-Vis) Spectrometry

UV-Vis spectra were obtained in a V-730 Spectrophotometer (JASCO – Japan), in the 190 - 800 nm wavelength range. Optical band gap energy (E<sub>g</sub>) was determined from absorbance versus wavelength data through Mott and Davis Equation 1<sup>[21]</sup>:

$$\alpha hv = C(hv - E_g)^n \quad (1)$$

in which α is the absorbance coefficient calculated from the absorbance-film thickness ratio<sup>[22]</sup>, C is a constant related to sample structure, E<sub>g</sub> is the optical band-gap energy, h is the Plank's constant, and n is the electronic transition index, varying from 1/2 to 3/2 for direct transitions, or from 2 to 3 for indirect transitions, depending on whether allowed or forbidden, respectively<sup>[23]</sup>. Previous works attributed n = 1/2<sup>[23,24]</sup> to PVA, as it exhibits allowed direct transitions. E<sub>g</sub> values were obtained from (αhv)<sup>2</sup> versus hv plot, by linear extrapolation of the curves to zero absorption value. E<sub>g</sub> is related to the number of carbon atoms per carbonaceous cluster in the PVA matrix by Equation 2<sup>[11]</sup>:

$$E_g = \frac{34.3}{\sqrt{M}} \quad (2)$$

Here, M is the carbon atoms number per cluster.

The exponential part of the absorption coefficient curve is called the Urbach tail. This tail appears in disordered or

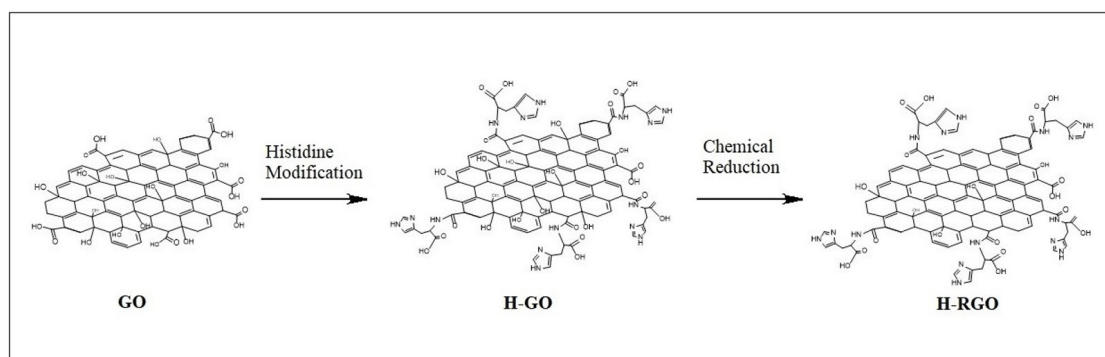


**Figure 1.** Scheme for histidine-modified reduced GO (H-RGO).

poorly crystalline materials as these materials present localized states extended in the band gap. The spectral dependence of  $\alpha$  and photon energy ( $h\nu$ ) is given by Equation 3<sup>[11,22]</sup>:

$$\alpha = \alpha_0 e^{(h\nu/E_u)} \quad (3)$$

where  $\alpha_0$  is a constant and  $E_u$  is the Urbach energy, which is interpreted as the width of the tails of localized states in the band gap and, in general, represents the degree of disorder and irregularities in the amorphous semiconductors<sup>[25]</sup>.

### 3.4 Electrical conductivity determinations

Superficial electrical conductivity ( $\sigma$ ) calculations of composite films were made from electrical resistance ( $R'$ ) measurements performed in an Electrometer (KEITHLEY 6517B model). Adapted Moon and Spencer Equation<sup>[26]</sup> was used to calculate  $\sigma$  (Equation 4):

$$\sigma = \frac{d \left( \cos^{-1} d/d_0 \right)}{2.27 R' t^2} \quad (4)$$

where  $t$  = sample thickness,  $d$  = distance between contacts,  $d_0$  = diameter of contacts.

## 4. Results and Discussions

### 4.1 FTIR analysis

Figure 2 shows FTIR-ATR spectra for GO, H-GO, and H-RGO. For the GO spectrum, the broad band around 3200  $\text{cm}^{-1}$  is typical of hydrogen-bonded carboxyl OH group stretching<sup>[27]</sup>. The band around 1713  $\text{cm}^{-1}$  is attributed to carbonyl stretching, while the band at 1041  $\text{cm}^{-1}$  is attributed to C-OH stretching<sup>[18]</sup>. The vibrations of the unoxidized graphitic skeleton occur at 1618  $\text{cm}^{-1}$ <sup>[27]</sup>. These data suggest effective graphite chemical oxidation. After superficial covalent modification with histidine, the product H-GO exhibited carboxylate group symmetrical

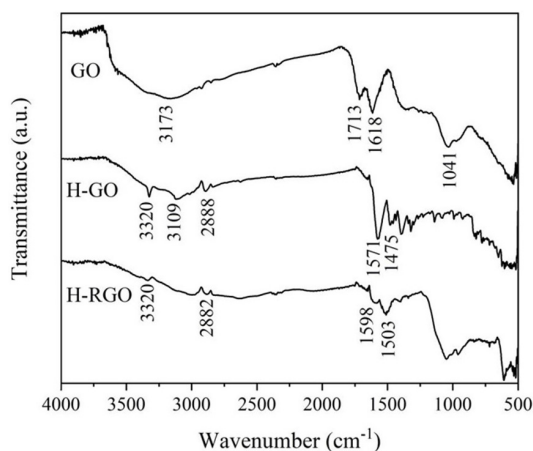


**Figure 2.** FTIR spectra of graphene oxide (GO), histidine-modified graphene oxide (H-GO), and histidine-modified reduced graphene oxide (H-RGO).

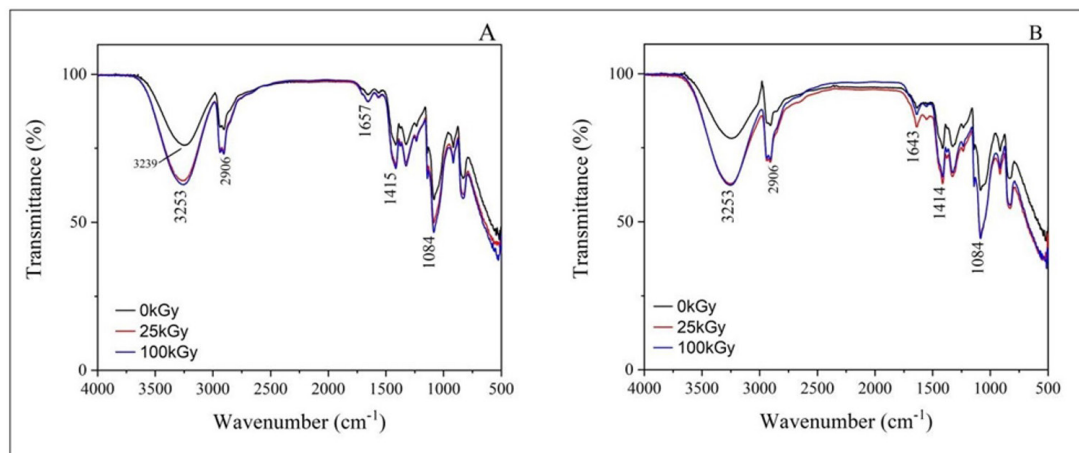
stretching vibrations (1475  $\text{cm}^{-1}$ )<sup>[28]</sup>. Due to NaOH treatment during the modification process, a decrease in the relative intensity of OH broadband in the 3600-2600  $\text{cm}^{-1}$  region could be noticed<sup>[29]</sup>. At higher wavenumbers, the N-H stretching vibration single band appears at 3320  $\text{cm}^{-1}$ , evidencing covalent bonding between histidine and GO. Additional evidence of histidine presence was observed in the 3108  $\text{cm}^{-1}$  band, attributed to the imidazole ring =C-H stretching vibration<sup>[30]</sup>, in the 2888  $\text{cm}^{-1}$  band, associated with histidine aliphatic  $\text{CH}_2$  stretching; and in the band at 1571  $\text{cm}^{-1}$ , corresponding to the imidazole ring's skeleton vibration<sup>[31]</sup>. After reduction, H-RGO showed even fewer FTIR-detectable oxygen groups. N-H stretching at 3320  $\text{cm}^{-1}$ , and the aliphatic C-H stretching at 2880  $\text{cm}^{-1}$  were still present, but with lower intensity probably due to histidine detachment after the reduction process. The presence of bands in 1598 and 1503  $\text{cm}^{-1}$  in H-RGO might be associated with the restoration of graphene-conjugated lattice, as reported by Pfaffeneder-Kmen et al.<sup>[32]</sup> for in-situ ATR-FTIR analysis of GO electrochemical reduction.

Figure 3 shows FTIR spectra for PVA and H-RGO nanocomposites. PVA data are in accordance with previous reports<sup>[33,34]</sup>. A broad band centered in 3239  $\text{cm}^{-1}$  was attributed to OH groups stretching and peaks around 2900  $\text{cm}^{-1}$  were attributed to CH asymmetrical stretching vibrations. Peaks at around 1657, 1415, and 1084  $\text{cm}^{-1}$  were assigned to C=O, C-H, and C-O stretch vibration, respectively. C=O groups are related to residual acetate groups after partial PVA hydrolysis. The spectra of composites do not significantly differ from the spectrum of PVA. The irradiated samples exhibited more intense absorption bands for oxygenated groups in both PVA and H-RGO samples. This suggests that irradiation-induced oxidation occurred, regardless of the presence of H-RGO filler. The increase in the intensity of the C-O bands suggests the presence of free radicals due to the interaction of ionizing radiation with PVA. These radicals can interact with OH groups leading to the formation of bonds between the polymer chains, which leads to crosslinking, an expected behavior for PVA matrices<sup>[35,36]</sup>.

### 4.2 Thermal analysis and determination of activation energy

Graphene derivatives GO and H-RGO, the PVA matrix, and the PVA/H-RGO were analyzed for their thermal behavior and thermograms are shown in Figure 4. GO has a significant mass loss (approximately 13%) below 100  $^{\circ}\text{C}$ , attributed to the removal of water from the material, which is known for its hydrophilic nature. The first stage of GO degradation begins around 200  $^{\circ}\text{C}$  and is associated with the decomposition of surface oxygenated functional groups, and the graphite residue does not degrade until 800  $^{\circ}\text{C}$ <sup>[18]</sup>.

H-RGO presents a more stable behavior up to 240  $^{\circ}\text{C}$  since most of its oxygenated functional groups are removed during chemical reduction. Then, the material underwent fast thermal degradation and lost almost 70% of its mass. PVA thermogram initially shows a slight loss of mass below 100  $^{\circ}\text{C}$ , attributed to the evaporation of water absorbed during film formation. It is observed that PVA, as reported in the literature<sup>[37]</sup>, presented two stages of thermal degradation. The first stage took place



**Figure 3.** FTIR spectra for PVA (A) and (B) PVA/H-RGO (0.5 wt%), unirradiated or-gamma-irradiated at 25 or 100 kGy doses.

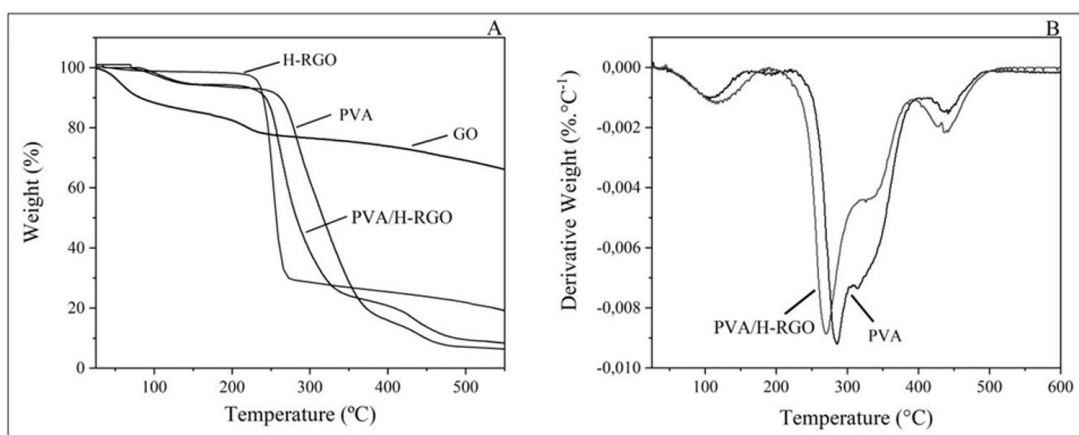


**Figure 4.** (A) Thermograms of GO, H-RGO, PVA and PVA/H-RGO composite; (B) First Derivative thermograms for PVA and PVA/H-RGO films.

around 264 °C when the elimination of hydroxyl side groups, main chain scissions, and formation of volatile compounds happened, leading to a loss of 76% of the polymer mass. The second stage, with a less significant mass loss (7%) initiated around 424 °C, is related to the elimination of newly formed compounds and continued removal of residual acetate groups from the polymerization starting material<sup>[37]</sup>. With the addition of the filler to the polymer matrix, only a decrease of 15.2 °C in the initial temperature ( $T_{\text{onset}}$ ) of the first degradation stage could be noticed, indicating nanocomposite thermal stability after the insertion of H-RGO filler. After irradiation, the PVA matrix underwent small changes in its thermal degradation steps, while PVA/H-RGO presented the same degradation steps, even after exposure to 100 kGy dose. It is clear that H-RGO, when embedded into the PVA matrix promotes radiolytic protection to the nanocomposite system. All data for initial temperature ( $T_{\text{onset}}$ ), temperature of maximum degradation rate ( $T_{\text{max}}$ ), and mass loss percentage ( $\Delta m$ ) at each degradation step are shown in Table 1.

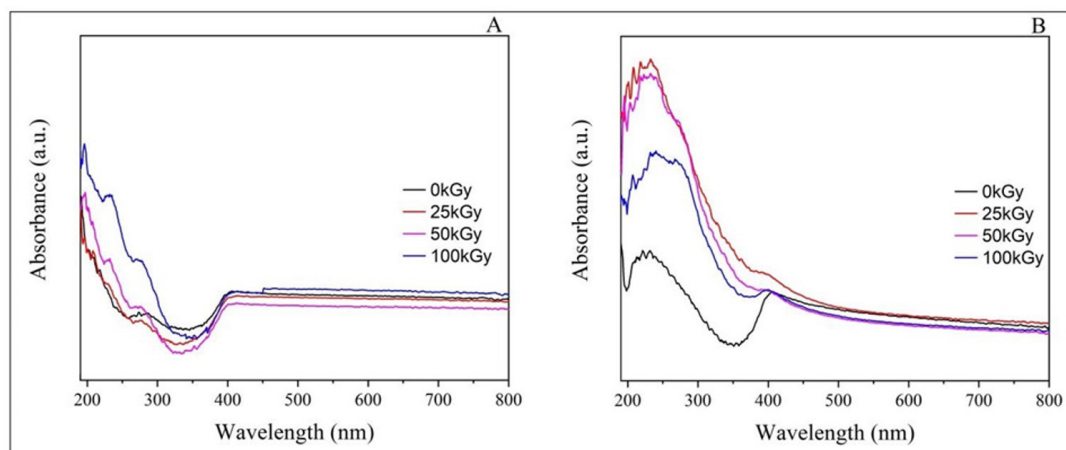
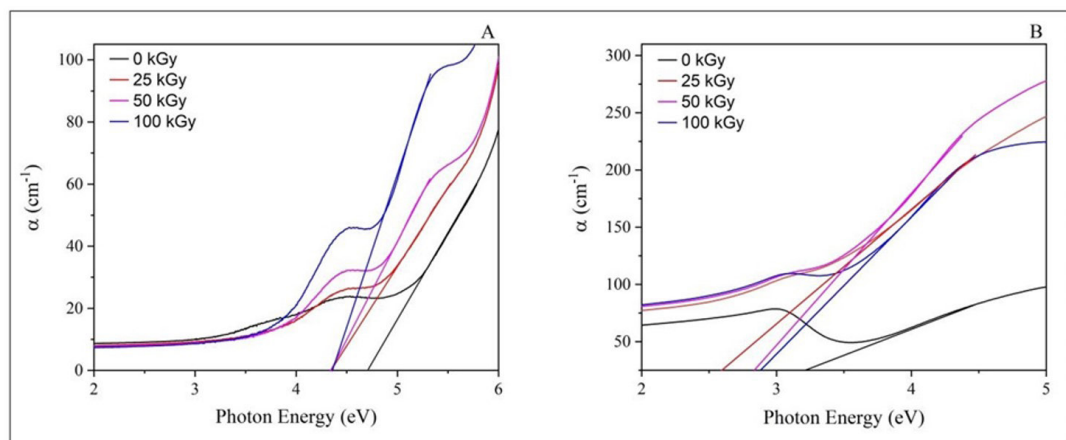
#### 4.3 UV-Vis analysis – optical properties study

Figure 5 shows UV-Vis spectra for PVA (5A) and PVA/H-RGO nanocomposite (5B), before and after irradiation. PVA transparency to visible light allowed low absorbance in the 400 – 800 nm region. PVA/H-RGO nanocomposite films presented good transparency, with absorbance around 0.4 in the same region. After irradiation, PVA films began to gradually exhibit an absorption peak around 230 and 270 nm (UV region), indicating the formation of C=O chromophores. In the nanocomposite, this peak appears centered at 230 nm, indicating that the presence of H-RGO might facilitate the processes of splitting C-H and O-H bonds, resulting in the formation of C=O groups during gamma irradiation.

UV-Vis analysis allows the study of the optical band gap of PVA films and their composites from parameters taken from absorption *versus* wavelength spectra. Absorption coefficient ( $\alpha$ ), and photon energy ( $h\nu$ ) were determined considering films with 10 $\mu\text{m}$  in thickness. Figure 6 shows the optical absorption coefficient *versus* photon energy

**Table 1.** Thermogravimetry analysis data for GO, H-RGO, unirradiated and gamma-irradiated films.

System	First Stage			Second Stage		
	$T_{\text{onset}}$ (°C)	$T_{\text{max}}$ (°C)	$\Delta m$ (%)	$T_{\text{onset}}$ (°C)	$T_{\text{max}}$ (°C)	$\Delta m$ (%)
GO	202.8 ± 3.6	220.3 ± 3.0	13.1 ± 0.9	-	-	-
H-RGO	244.0 ± 2.1	257.5 ± 3.9	68.3 ± 0.2	-	-	-
PVA	263.8 ± 3.4	278.0 ± 9.5	75.6 ± 1.8	424.4 ± 7.6	441.2 ± 0.9	7.0 ± 0.2
PVA (100 kGy)	242.1 ± 0.4	265.0 ± 0.0	58.4 ± 0.5	426.9 ± 0.3	437.7 ± 0.0	18.9 ± 0.2
PVA/H-RGO	248.6 ± 1.3	265.6 ± 3.7	68.4 ± 0.3	421.5 ± 5.7	438.2 ± 4.3	11.0 ± 1.8
PVA/H-RGO (100 kGy)	249.8 ± 4.7	264.8 ± 5.9	66.8 ± 3.8	431.8 ± 0.2	453.7 ± 4.0	10.5 ± 2.3

**Figure 5.** (A) PVA and (B) PVA/H-RGO (0.5 wt%) nanocomposite films UV-Vis spectra for unirradiated or gamma-irradiated (25, 50, and 100 kGy) samples.**Figure 6.** Optical absorption coefficient ( $\alpha$ ) versus photon energy for (A) PVA and (B) PVA/H-RGO, at 0, 25, 50, and 100 kGy doses.

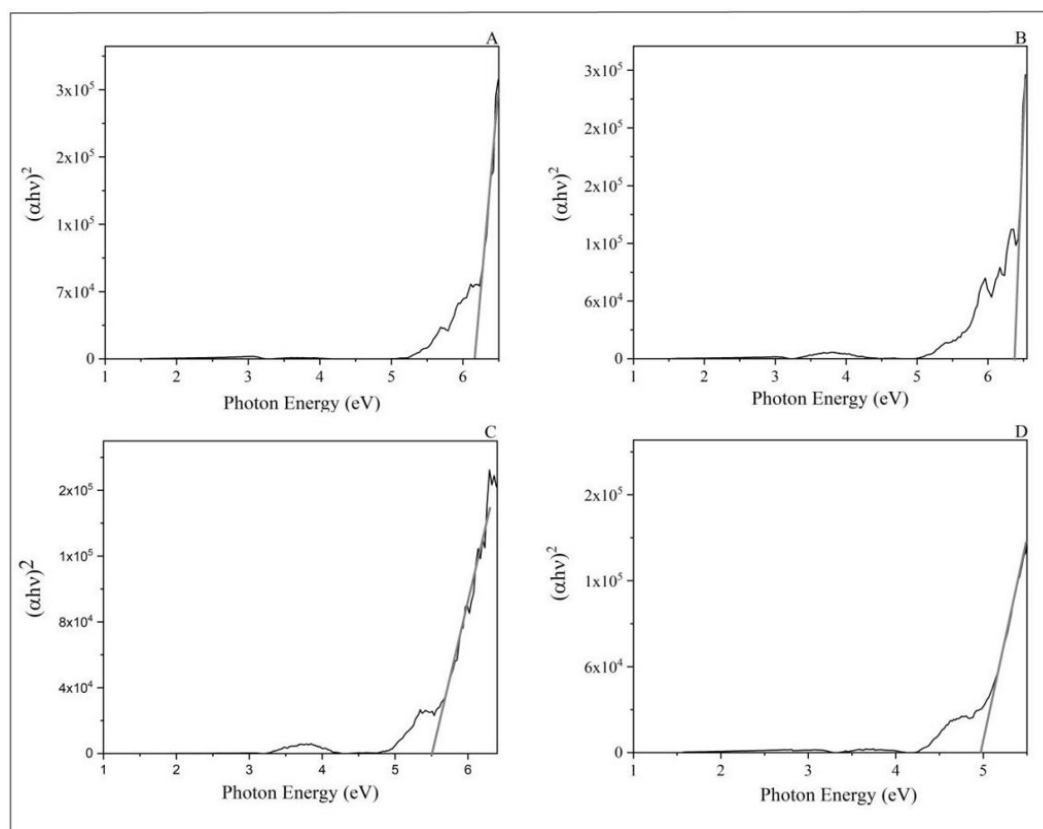
curves for PVA and PVA/H-RGO nanocomposite films. The absorption edge ( $E_d$ ) is determined by extrapolating the linear part of  $\alpha$  versus  $h\nu$  (eV) curves to zero absorption value<sup>[23]</sup>. It is observed that the absorption edge is reduced from 4.89 to 3.42 after adding H-RGO nanofillers into the PVA matrix (Table 2). Also, gamma irradiation on polymer systems promoted the reduction of  $E_d$  values in both PVA and PVA/H-RGO nanocomposite.

Curves obtained from  $(\alpha h\nu)^2$  versus  $h\nu$  plots were used for drawing a tangential line as an extrapolation of the curve linear region. For  $(\alpha h\nu)^2 = 0$ , optical band gap energy values ( $E_g$ ) were determined. These curves, as well as their linear extrapolations, are presented in Figures 7 and 8, for PVA and PVA/H-RGO films, respectively.

$E_g$  value (Table 2) for PVA was 6.20 eV, which is in agreement with previous reports<sup>[34]</sup>. The addition of H-RGO

**Table 2.** Optical parameters for PVA and PVA/H-RGO (0.5 wt%) composites before and after gamma irradiation.

System	Dose (kGy)	Absorption edge $E_d$ (eV)	Optical band gap $E_g$ (eV)	Urbach energy $E_u$ (eV)	Mobility band gap energy $E_g + E_u$	Number of carbon per cluster M
PVA	0	$4.78 \pm 0.07$	$6.20 \pm 0.74$	$2.62 \pm 0.13$	$8.82 \pm 0.87$	31
	25	$4.31 \pm 0.11$	$6.37 \pm 0.56$	$1.78 \pm 0.10$	$8.15 \pm 0.66$	29
	50	$4.28 \pm 0.05$	$5.49 \pm 0.23$	$1.00 \pm 0.04$	$6.49 \pm 0.27$	39
	100	$4.18 \pm 0.20$	$4.96 \pm 0.17$	$0.31 \pm 0.03$	$5.27 \pm 0.20$	43
PVA / H-RGO	0	$3.42 \pm 0.05$	$3.76 \pm 0.05$	$0.35 \pm 0.01$	$4.11 \pm 0.06$	83
	25	$2.73 \pm 0.14$	$3.68 \pm 0.04$	$0.32 \pm 0.01$	$4.00 \pm 0.05$	87
	50	$2.93 \pm 0.35$	$3.69 \pm 0.06$	$0.32 \pm 0.01$	$4.01 \pm 0.07$	86
	100	$3.01 \pm 0.13$	$3.52 \pm 0.08$	$0.19 \pm 0.02$	$3.71 \pm 0.10$	95

**Figure 7.** Optical band gap ( $E_g$ ) of PVA films after irradiation with doses of (A) 0 kGy, (B) 25 kGy, (C) 50 kGy and (D) 100 kGy.

into the PVA matrix decreases  $E_g$  values from 6.20 to 3.76 eV, turning this novel polymer nanocomposite into a useful material for optoelectronic applications. This decrease might be associated with an increase in the density of localized states in the band gap of the PVA matrix, generating new energy levels between the bands of the highest occupied molecular orbital (HOMO) and the lowest unoccupied molecular orbital (LUMO), due to an increase in disorder level after H-RGO filler incorporation<sup>[34]</sup>.

Urbach energy ( $E_u$ ) values were found from the slope of the linear region of the  $\ln(\alpha)$  versus  $h\nu$  plot (Figure 9).  $E_u$  values decrease from 2.62 eV (PVA) to 0.35 eV (PVA/H-RGO).

In general, the energy difference between localized states in the valence band and extended states in the conduction band represents  $E_g$ , and the sum  $E_g + E_u$  represents the mobility band gap energy<sup>[34,38]</sup>. Thus, the decrease in the mobility band gap energy values of the gamma-irradiated PVA, as seen in Table 2, can be explicated by the formation of radiolytic events such as main chain scissions, free radicals, and oxidation, which promote disorder and imperfections in the structure of the polymer matrix. These events lead to the creation of new localized states of various depths in the forbidden band energy, which, in general, contributes to the decrease in optical band gap energy. It is worth

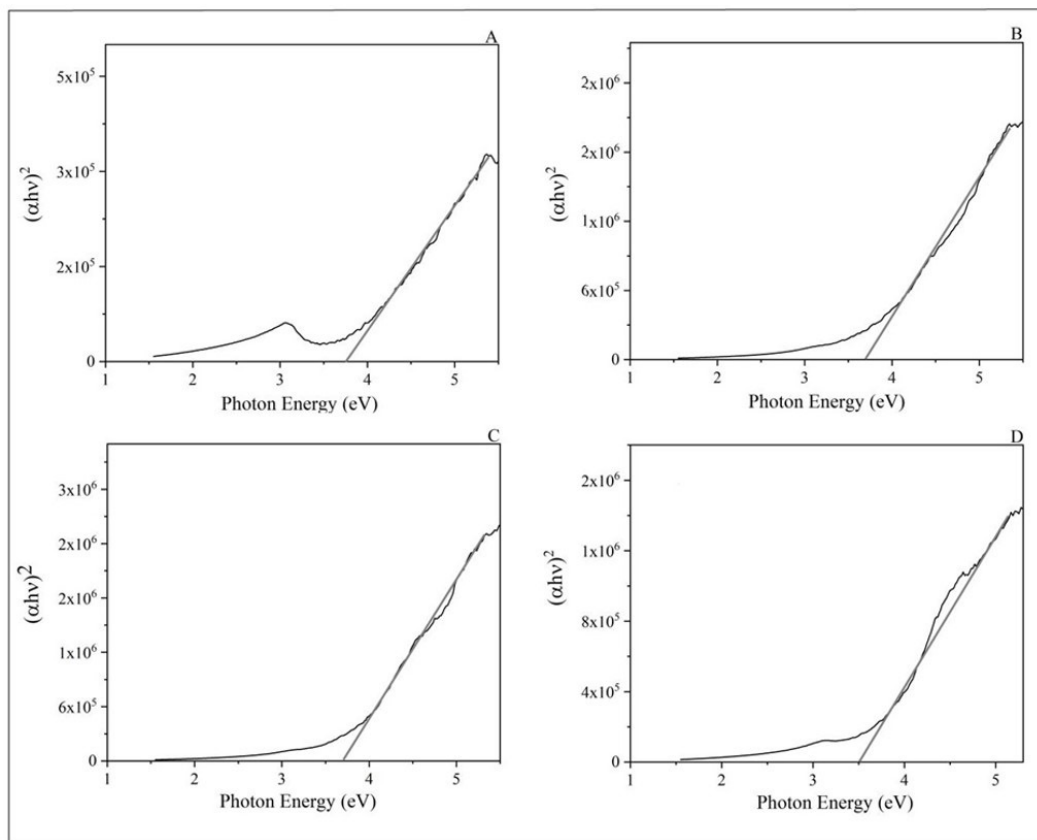


**Figure 8.** Optical band gap ( $E_g$ ) of PVA/H-RGO (0.5 wt%) nanocomposite films after irradiation with doses of (A) 0 kGy, (B) 25 kGy, (C) 50 kGy and (D) 100 kGy.

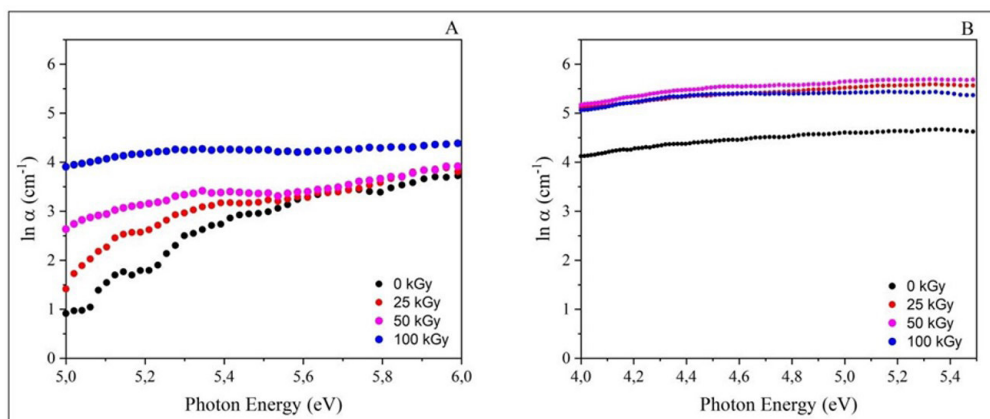


**Figure 9.**  $\ln(\alpha)$  versus photon energy plot for (A) PVA and (B) PVA/H-RGO (0.5 wt%), at 0, 25, 50, and 100 kGy doses.

mentioning that the reduction of  $T_{\text{onset}}$  and  $T_{\text{max}}$  in the first stage of gamma-irradiated PVA thermal degradation is characteristic of main chain scission effects (Table 1). However, the mobility band gap energy of the PVA/H-RGO nanocomposite did not significantly change with gamma irradiation. It is well known that aromatic structures promote radiolytic protection on polymer systems<sup>[39]</sup>, as they disperse

excess energy through delocalized electrons in the aromatic system. It is possible to infer that H-RGO, a filler that bears a number of aromatic fused rings into its graphene structure, might stabilize PVA against gamma-irradiation damages up to 50 kGy dose.

The number of carbon atoms per carbonaceous grouping,  $M$ , for the unirradiated PVA matrix was 31,

and for the nanocomposite increased to 83. This increase in  $M$  values is due to the conjugation of PVA hydroxyl groups and hydrogen bond-forming groups present in H-RGO, such as secondary amino (N-H), imidazole, and carboxylate from histidine (see FTIR analysis, section 4.1), along with possible residual hydroxyl and carboxy groups from incomplete graphene oxide reduction, among others. Abdelhamied et al.<sup>[23]</sup> reported a considerable increase in  $M$  when pristine PVA was filled with polyaniline emeraldine hydrochloric salt (PANI-HCl). While PVA presented  $M$  of 34.5, PVA/PANI-HCl (10 wt%) composites  $M$  values were found to be around 58. Noticeably, both fillers, PANI-HCl and H-RGO are able to form strong intermolecular interactions with the PVA matrix. Nevertheless, H-RGO was used in a much smaller concentration (0.5 wt%) than PANI-HCl (10 wt%)<sup>[40]</sup>. Optical parameters of PVA and PVA/H-RGO films were significantly affected by gamma irradiation, as shown in Table 2. Nevertheless, these radiation-induced modifications on optical parameters do not exclude PVA/H-RGO nanocomposites from optoelectronic applications, since the parameters remain within the expected range, as also observed by other researchers<sup>[17,19]</sup>.

#### 4.4 Electrical properties

PVA is an electrical insulator material, and its conductivity is around  $10^{-11}$  S.cm<sup>-1</sup>. With the addition of H-RGO, the composite showed electrical conductivity 5 orders of magnitude higher, reaching semiconductivity with  $10^{-6}$  S.cm<sup>-1</sup> (Figure 10). PVA and PVA/H-RGO films were exposed to gamma irradiation doses of 25, 50, and 100 kGy. An increase from  $10^{-11}$  S.cm<sup>-1</sup> to  $10^{-9}$  S.cm<sup>-1</sup> after 25 kGy dose was observed for PVA. Gamma-irradiated PVA/H-RGO nanocomposite reached  $10^{-4}$  S.cm<sup>-1</sup> in conductivity, after the same dose. It is worth noting that the range  $10^{-6} < \sigma < 10^{-1}$  S.cm<sup>-1</sup> characterizes semiconductor materials<sup>[41]</sup>. According to Prabha and Jayanna<sup>[42]</sup>, the increase in polymer conductivity is related to the presence of free ions connected to the polymer chain. Thus, radiation-induced polymer radiolytic products might contribute to increased electrical conductivity of the polymer system. PVA/H-RGO nanocomposites underwent considerable change in electrical conductivity after gamma irradiation. These materials might

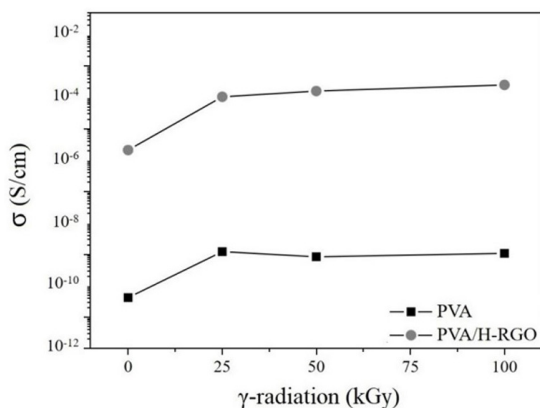


**Figure 10.** Surface electrical conductivity versus gamma-radiation dose for PVA or PVA/H-RGO (0.5 wt%) nanocomposite films.

play important roles in environments exposed to ionizing radiation, such as outer space or nuclear power plants.

## 5. Conclusions

The influence of gamma irradiation on graphene-based polymer nanocomposites was studied in the scope of their thermal, optical, and electrical properties. Graphene oxide, when chemically modified with histidine, a natural metabolite, and mildly reduced with cysteine, another natural metabolite H-RGO, and embedded into the PVA matrix promotes radiolytic protection to the nanocomposite system, since thermal parameters were not significantly changed by gamma irradiation. From the analysis of UV-Vis spectrophotometry was possible to obtain optical parameters for PVA and PVA/H-RGO composites. The optical band gap energy value found for PVA was 6.20 eV, this value decreased especially at higher doses of gamma irradiation. For the PVA/H-RGO nanocomposite films containing 0.5% filler, a significant decrease in the optical band gap from 6.20 to 3.76 eV took place. The mobility band gap energy of PVA/H-RGO nanocomposite films was not significantly changed with gamma doses up to 50 kGy. Additionally, PVA/H-RGO nanocomposite films presented electrical conductivity around  $10^{-6}$  S.cm<sup>-1</sup>, thus, being semiconducting materials. Thus, the modified graphene filler is a good alternative to impart electrical conductivity to the PVA matrix without interfering with relevant matrix physical properties, even after exposure to high doses of gamma irradiation. This novel polymer nanocomposite has great potential for optoelectronic, sensor, and avionics devices.

## 6. Author's Contribution

- **Conceptualization** – Thais Lima; Elmo Araújo; Patrícia Araújo.
- **Data curation** – Thais Lima; Filipe Diniz.
- **Formal analysis** – Thais Lima; Filipe Diniz.
- **Funding acquisition** – Elmo Araújo; Patrícia Araújo.
- **Investigation** – Thais Lima; Filipe Diniz.
- **Methodology** – Thais Lima; Elmo Araújo; Patrícia Araújo.
- **Project administration** – Elmo Araújo; Patrícia Araújo.
- **Resources** – Thais Lima; Filipe Diniz; Elmo Araújo; Patrícia Araújo.
- **Software** – NA.
- **Supervision** – Elmo Araújo; Patrícia Araújo.
- **Validation** – NA.
- **Visualization** – NA.
- **Writing – original draft** – Thais Lima; Filipe Diniz; Elmo Araújo; Patrícia Araújo.
- **Writing – review & editing** – Thais Lima; Filipe Diniz; Elmo Araújo; Patrícia Araújo.

## 7. Acknowledgements

The authors were grateful for the financial support from CNPq (Conselho Nacional de Pesquisa e Desenvolvimento

Científico e Tecnológico), CAPES (Coordenação de Aperfeiçoamento Pessoal de Nível Superior) and FACEPE (Fundação de Amparo à Ciência e Tecnologia de Pernambuco).

## 8. References

- Badawi, A. (2020). Engineering the optical properties of PVA/PVP polymeric blend in situ using tin sulfide for optoelectronics. *Applied Physics. A, Materials Science & Processing*, 126(5), 335. <http://doi.org/10.1007/s00339-020-03514-5>.
- Badawi, A., Alharthi, S. S., Mostafa, N. Y., Althobaiti, M. G., & Altalhi, T. (2019). Effect of carbon quantum dots on the optical and electrical properties of polyvinylidene fluoride polymer for optoelectronic applications. *Applied Physics. A, Materials Science & Processing*, 125(12), 858. <http://doi.org/10.1007/s00339-019-3160-1>.
- Karthikeyan, B., Hariharan, S., Mangalaraja, R. V., Pandiyarajan, T., Udayabhaskar, R., & Sreekanth, P. (2018). Studies on NiO-PVA composite films for opto-electronics and optical limiters. *IEEE Photonics Technology Letters*, 30(17), 1539-1542. <http://doi.org/10.1109/LPT.2018.2859042>.
- Fan, L., Wang, M., Zhang, Z., Qin, G., Hu, X., & Chen, Q. (2018). Preparation and characterization of PVA alkaline solid polymer electrolyte with addition of bamboo charcoal. *Materials*, 11(5), 679. <http://doi.org/10.3390/ma11050679>. PMID:29701694.
- Ali, F. M., Kersh, R. M., Sayed, M. A., & AbouDeif, Y. M. (2018). Evaluation of structural and optical properties of Ce<sup>3+</sup> ions doped (PVA/PVP) composite films for new organic semiconductors. *Physica B, Condensed Matter*, 538, 160-166. <http://doi.org/10.1016/j.physb.2018.03.031>.
- Otaguro, H., Lima, L. F. C. P., Parra, D. F., Lugão, A. B., Chinelatto, M. A., & Canevarolo, S. V. (2010). High-energy radiation forming chain scission and branching in polypropylene. *Radiation Physics and Chemistry*, 79(3), 318-324. <http://doi.org/10.1016/j.radphyschem.2009.11.003>.
- Yoshiga, A., Otaguro, H., Parra, D. F., Lima, L. F. C. P., & Lugão, A. B. (2009). Controlled degradation and crosslinking of polypropylene induced by gamma radiation and acetylene. *Polymer Bulletin*, 63(3), 397-409. <http://doi.org/10.1007/s00289-009-0102-7>.
- Xu, Z., Huang, Y., Zhang, C., Liu, L., Zhang, Y., & Wang, L. (2007). Effect of  $\gamma$ -ray irradiation grafting on the carbon fibers and interfacial adhesion of epoxy composites. *Composites Science and Technology*, 67(15-16), 3261-3270. <http://doi.org/10.1016/j.compscitech.2007.03.038>.
- Araújo, E. S., Khoury, H. J., & Silveira, S. V. (1998). Effects of gamma-irradiation on some properties of duralon polycarbonate. *Radiation Physics and Chemistry*, 53(1), 79-84. [http://doi.org/10.1016/S0969-806X\(97\)00300-9](http://doi.org/10.1016/S0969-806X(97)00300-9).
- Sunitha, V. R., & Radhakrishnan, S. (2020). Gamma irradiation effects on conductivity and dielectric behaviour of PEO-based nano-composite polymer electrolyte systems. *Polymer Bulletin*, 77(2), 655-670. <http://doi.org/10.1007/s00289-019-02770-7>.
- Chahal, R. P., Mahendia, S., Tomar, A. K., & Kumar, S. (2012).  $\gamma$ -Irradiated PVA/Ag nanocomposite films: materials for optical applications. *Journal of Alloys and Compounds*, 538, 212-219. <http://doi.org/10.1016/j.jallcom.2012.05.085>.
- Huang, G., Ni, Z., Chen, G., & Zhao, Y. (2016). The influence of irradiation and accelerated aging on the mechanical and tribological properties of the graphene oxide/ultra-high-molecular-weight polyethylene nanocomposites. *International Journal of Polymer Science*, 2016, 2618560. <http://doi.org/10.1155/2016/2618560>.
- Zhang, D., Yang, S., Chen, Y., Liu, S., Zhao, H., & Gu, J. (2018). <sup>60</sup>Co  $\gamma$ -ray irradiation crosslinking of chitosan/graphene oxide composite film: swelling, thermal stability, mechanical, and antibacterial properties. *Polymers*, 10(3), 294. <http://doi.org/10.3390/polym10030294>. PMID:30966329.
- Ramya, J. R., Arul, K. T., Sathiamurthi, P., Nivethaa, E. A. K., Baskar, S., Amudha, S., Mohana, B., Elayaraja, K., Veerla, S. C., Asokan, K., & Kalkura, S. N. (2019). Gamma irradiated poly (methyl methacrylate)-reduced graphene oxide composite thin films for multifunctional applications. *Composites. Part B, Engineering*, 163, 752-760. <http://doi.org/10.1016/j.compositesb.2019.01.041>.
- Paradossi, G., Cavalieri, F., Chiessi, E., Spagnoli, C., & Cowman, M. K. (2003). Poly(vinyl alcohol) as versatile biomaterial for potential biomedical applications. *Journal of Materials Science. Materials in Medicine*, 14(8), 687-691. <http://doi.org/10.1023/A:1024907615244>. PMID:15348409.
- Hummers, W. S., Jr., & Offeman, R. E. (1958). Preparation of graphitic oxide. *Journal of the American Chemical Society*, 80(6), 1339. <http://doi.org/10.1021/ja01539a017>.
- Geng, Y., Wang, S. J., & Kim, J.-K. (2009). Preparation of graphite nanoplatelets and graphene sheets. *Journal of Colloid and Interface Science*, 336(2), 592-598. <http://doi.org/10.1016/j.jcis.2009.04.005>. PMID:19414181.
- Mallakpour, S., Abdolmaleki, A., & Borandeh, S. (2014). Covalently functionalized graphene sheets with biocompatible natural amino acids. *Applied Surface Science*, 307, 533-542. <http://doi.org/10.1016/j.apsusc.2014.04.070>.
- Lima, T. B. S., Silva, V. O., Araujo, E. S., & Araujo, P. L. B. (2019). Polymer nanocomposites of surface-Modified graphene I: thermal and electrical properties of poly(vinyl alcohol)/amino acid-functionalized graphene. *Macromolecular Symposia*, 383(1), 1800051. <http://doi.org/10.1002/masy.201800051>.
- Chen, D., Li, L., & Guo, L. (2011). An environment-friendly preparation of reduced graphene oxide nanosheets via amino acid. *Nanotechnology*, 22(32), 325601. <http://doi.org/10.1088/0957-4484/22/32/325601>. PMID:21757797.
- Davis, E. A., & Mott, N. F. (1970). Conduction in non-crystalline systems V. Conductivity, optical absorption and photoconductivity in amorphous semiconductors. *Philosophical Magazine*, 22(179), 903-922. <http://doi.org/10.1080/14786437008221061>.
- Muhammad, F. F., Aziz, S. B., & Hussein, S. A. (2015). Effect of the dopant salt on the optical parameters of PVA:NaNO<sub>3</sub> solid polymer electrolyte. *Journal of Materials Science Materials in Electronics*, 26(1), 521-529. <http://doi.org/10.1007/s10854-014-2430-0>.
- Abdelhamied, M. M., Atta, A., Abdelreheem, A. M., Farag, A. T. M., & El Okr, M. M. (2020). Synthesis and optical properties of PVA/PANI/Ag nanocomposite films. *Journal of Materials Science Materials in Electronics*, 31(24), 22629-22641. <http://doi.org/10.1007/s10854-020-04774-w>.
- Selvi, J., Mahalakshmi, S., Parthasarathy, V., Hu, C., Lin, Y.-F., Tung, K.-L., Anbarasan, R., & Annie, A. A. (2019). Optical, thermal, mechanical properties, and non-isothermal degradation kinetic studies on PVA/CuO nanocomposites. *Polymer Composites*, 40(9), 3737-3748. <http://doi.org/10.1002/pc.25235>.
- Sharma, P., & Katyal, S. C. (2008). Effect of tin addition on the optical parameters of thermally evaporated As-Ge thin films. *Materials Chemistry and Physics*, 112(3), 892-897. <http://doi.org/10.1016/j.matchemphys.2008.07.035>.
- Moon, P., & Spencer, D. E. (1961) *Field Theory for Engineers*. Princeton: D. Van Nostrand Company, Inc.. <http://doi.org/10.1119/1.1937573>.
- Stankovich, S., Piner, R. D., Nguyen, S. T., & Ruoff, R. S. (2006). Synthesis and exfoliation of isocyanate-treated graphene

- oxide nanoplatelets. *Carbon*, 44(15), 3342-3347. <http://doi.org/10.1016/j.carbon.2006.06.004>.
28. Zhang, Y., Li, H., Xi, B., Che, Y., & Zheng, J. (2008). Growth and characterization of L-histidine nitrate single crystal, a promising semiorganic NLO material. *Materials Chemistry and Physics*, 108(2-3), 192-195. <http://doi.org/10.1016/j.matchemphys.2007.09.006>.
  29. Rajaura, R. S., Sharma, V., Ronin, R. S., Gupta, D. K., Srivastava, S., Agrawal, K., & Vijay, Y. K. (2017). Synthesis, characterization and enhanced antimicrobial activity of reduced graphene oxide-zinc oxide nanocomposite. *Materials Research Express*, 4(2), 025401. <http://doi.org/10.1088/2053-1591/aa5bff>.
  30. Viruthagiri, G., Praveen, P., Mugundan, S., & Anbuvaran, M. (2013). Growth and characterization of L-histidine doped thiourea single crystals by slow evaporation method. *Indian Journal of Advances in Chemical Science*, 1(4), 193-200. Retrieved in 2023, December 21, from <http://ijacs-kros.com/articles/IJACS-M29.pdf>
  31. Epishina, L. V., Slovetskii, V. I., Osipov, V. G., Lebedev, O. V., Khmel'nitskii, L. I., Sevost'yanova, V. V., & Novikova, T. S. (1967). Infrared spectra and the structure of salts of imidazoles. *Chemistry of Heterocyclic Compounds*, 3(2), 570-575. <http://doi.org/10.1007/BF00481609>.
  32. Pfaffeneder-Kmen, M., Falcon Casas, I., Naghilou, A., Trettenhahn, G., & Kautek, W. (2017). A multivariate curve resolution evaluation of an in-situ ATR-FTIR spectroscopy investigation of the electrochemical reduction of graphene oxide. *Electrochimica Acta*, 255, 160-167. <http://doi.org/10.1016/j.electacta.2017.09.124>.
  33. Xue, B., Ji, L., Deng, J., & Zhang, J. (2016). In situ FTIR spectroscopy study on the rapid dissolution process of modified poly(vinyl alcohol). *Journal of Polymer Research*, 23(10), 209. <http://doi.org/10.1007/s10965-016-1100-8>.
  34. Abdullah, O. G., Aziz, S. B., & Rasheed, M. A. (2016). Structural and optical characterization of PVA:KMnO<sub>4</sub> based solid polymer electrolyte. *Results in Physics*, 6, 1103-1108. <http://doi.org/10.1016/j.rinp.2016.11.050>.
  35. Ali, Z. I., Ali, F. A., & Hosam, A. M. (2009). Effect of electron beam irradiation on the structural properties of PVA/V2O<sub>5</sub> xerogel. *Spectrochimica Acta. Part A: Molecular and Biomolecular Spectroscopy*, 72(4), 868-875. <http://doi.org/10.1016/j.saa.2008.12.013>. PMID:19157963.
  36. Kamoun, E. A., Chen, X., Mohy Eldin, M. S., & Kenawy, E.-R. S. (2015). Crosslinked poly(vinyl alcohol) hydrogels for wound dressing applications: a review of remarkably blended polymers. *Arabian Journal of Chemistry*, 8(1), 1-14. <http://doi.org/10.1016/j.arabjc.2014.07.005>.
  37. Ravari, F., Noori, M., & Ehsani, M. (2019). Thermal stability and degradation kinetic studies of PVA/RGO using the model-fitting and isoconversional (model-free) methods. *Fibers and Polymers*, 20(3), 472-480. <http://doi.org/10.1007/s12221-019-8606-8>.
  38. Sbeih, S. A., & Zihlif, A. M. (2009). Optical and electrical properties of kaolinite/polystyrene composite. *Journal of Physics. D, Applied Physics*, 42(14), 145405. <http://doi.org/10.1088/0022-3727/42/14/145405>.
  39. Silva, F. F., Aquino, K. A. S., & Araujo, E. S. (2008). Effects of gamma irradiation on poly(vinyl chloride)/polystyrene blends: investigation of radiolytic stabilization and miscibility of the mixture. *Polymer Degradation & Stability*, 93(12), 2199-2203. <http://doi.org/10.1016/j.polymdegradstab.2008.07.024>.
  40. Heeger, A. J. (2001). Nobel Lecture: Semiconducting and metallic polymers: the fourth generation of polymeric materials. *Reviews of Modern Physics*, 73(3), 681-700. <http://doi.org/10.1103/RevModPhys.73.681>.
  41. Pang, H., Xu, L., Yan, D.-X., & Li, Z.-M. (2014). Conductive polymer composites with segregated structures. *Progress in Polymer Science*, 39(11), 1908-1933. <http://doi.org/10.1016/j.progpolymsci.2014.07.007>.
  42. Prabha, K., & Jayanna, H. S. (2015). Study the frequency dependence of dielectric properties of gamma irradiated PVA<sub>(1-x)</sub>PS<sub>x</sub> polymer blends. *Open Journal of Polymer Chemistry*, 5(4), 47-54. <http://doi.org/10.4236/ojpcem.2015.54006>.

Received: Dec. 21, 2023

Revised: Sept. 25, 2024

Accepted: Oct. 28, 2024